Journal of Structural Geology 33 (2011) 1477–1490

Contents lists available at ScienceDirect

Journal of Structural Geology

journal homepage: www.elsevier.com/locate/jsg

Conditions and implications for compaction band formation in the Navajo Sandstone, Utah

Haakon Fossen [a,b,*], Richard A. Schultz [c], Anita Torabi [a]

[a] Center for Integrated Petroleum Research, PO Box 7800 N, 5020 Bergen, Norway
[b] Department of Earth Science, University of Bergen, Allegaten 41, 5007 Bergen, Norway
[c] Geomechanics-Rock Fracture Group, Department of Geological Sciences and Engineering, 172, University of Nevada, Reno, NV 89557, USA

ARTICLE INFO

Article history:
Received 16 February 2011
Received in revised form
19 July 2011
Accepted 5 August 2011
Available online 16 August 2011

Keywords:
Compaction bands
Deformation bands
Strain localization
Navajo Sandstone
Permeability
Porosity

ABSTRACT

Observations from quartz-rich eolian Navajo Sandstone in the Buckskin Gulch site in southernmost Utah show that pure compaction bands only occur in sandstones where current porosity $> 0.29 \pm 3$, permeability $> 10 \pm 7$ darcy, and grain size > 0.4 mm – properties restricted to the lower and most coarse-grained and well-sorted parts of grain flow units within the dune units. Hence a direct correlation between stratigraphy and band occurrence has been established that can be used to predict deformation band occurrences in similar sandstone reservoirs.

We show that the pure compaction bands formed perpendicular to a subhorizontal σ_1, bisecting conjugate sets of shear-enhanced compaction bands. The latter bands locally developed into shear-dominated bands that transect entire dune units, suggesting that an increase in the amount of simple shear promotes band propagation into less porous and permeable lithologies.

Stress considerations indicate that, as a continuous and overlapping sequence of events, pure compaction bands in quartz-rich Navajo Sandstone initiated at 10–20 MPa ($\sim$1 km depth), followed by shear-enhanced compaction bands that locally developed into more stratigraphically extensive shear-dominated bands. The rare combination of special lithologic and stress conditions may explain why pure compaction bands are rarely observed in naturally deformed sandstones.

1. Introduction

At low strains, porous sandstones tend to develop tabular strain localization features known as deformation bands (Schultz and Siddharthan, 2005; Aydin et al., 2006; Fossen et al., 2007). Kinematically, deformation bands range from isochoric shear bands to pure dilation bands on one extreme and pure compaction bands on the other (Cobbold, 1977). The most common type by far is *compactional* (or compactive) *shear bands*, i.e. shear bands involving an amount of band-perpendicular compaction that is clearly smaller than the band-parallel shear component. Less common are *shear-enhanced compaction bands*, defined by Eichhubl et al. (2010) as deformation bands with roughly equal amounts of shear and compaction. Such bands have been found in a few highly porous sandstones, where they have previously been referred to as compaction bands (e.g., Eichhubl et al., 2004; Sternlof et al., 2006; Saillet, 2009; Schultz, 2009).

Natural examples of *pure compaction* (and dilation) *bands*, i.e. bands with no shear displacement, seem to be quite uncommon, even though compaction bands have been produced in a range of physical experiments on highly porous sandstones (Olsson, 1999; Baud et al., 2004; DiGiovanni et al., 2007; Townend et al., 2008) and limestones (Baxevanis et al., 2006), and are found to constitute borehole breakout structures (Haimson, 2001). The only two field sites where pure compaction bands are common and well described are Buckskin Gulch in southern Utah (Mollema and Antonellini, 1996) and the Valley of Fire State Park area in southeastern Nevada (Sternlof et al., 2005), both located in the Jurassic eolian sandstones of southwestern USA. A key question that needs to be addressed is why compaction bands are so rare, or in other words, what are the conditions that promote their formation? A complete answer will necessarily involve a number of factors, of which lithologic properties (e.g., Mollema and Antonellini, 1996) and state and amount of stress (Schultz et al., 2010) are likely to be of major importance. In this paper we will focus on these two factors, and particularly on lithologic aspects through

* Corresponding author. Department of Earth Science, University of Bergen, Allegaten 41, 5007 Bergen, Norway. Tel.: +47 55583495; fax: +47 55583660.
E-mail address: haakon.fossen@geo.uib.no (H. Fossen).

0191-8141/$ – see front matter © 2011 Elsevier Ltd. All rights reserved.
doi:10.1016/j.jsg.2011.08.001

detailed structural and petrophysical observations of compaction bands and their host rocks in the Buckskin Gulch area, southern Utah, USA.

2. Geologic setting

The Buckskin Gulch is located in the easternmost part of the East Kaibab Monocline in southernmost Utah, 5–6 km north of the Utah-Arizona state line (Fig. 1). This monocline is one of several Laramide structures on the Colorado Plateau that formed in response to reactivation of pre-Laramide basement faults. The East Kaibab Monocline is generally thought to be controlled by a steep W-dipping reverse basement fault that is exposed in the Grand Canyon area where it appears to be a reactivated Precambrian normal fault (the Butte Fault; Davis and Bump, 2009). The monocline is an approximately N15E trending structure that makes a gentle bend around Buckskin Gulch to a locally more northeasterly orientation (Fig. 1). Minor faults that are oblique to the overall trend of the monocline are mapped north of Highway 89, and have been interpreted as a result of dextral strike–slip along the monocline (Tindall and Davis, 1999). However, we have not observed such faults, or any other structures indicating strike–slip movement, in the Buckskin Gulch area.

The Laramide orogeny is generally thought to have initiated around 70 Ma, lasting into the Eocene (e.g. Goldstrand, 1994; Dickinson, 2009). However, the onset of Laramide deformation in this area is considered by Tindall et al. (2010) to be reflected by synsedimentary structures in the upper Wahweap Formation. Radiometric dating of bentonite layers in this formation (Roberts et al., 2005) suggests that these earliest Laramide-related structures formed around 80–76 Ma.

The burial history of the Navajo Sandstone was constructed (Fig. 2) by using stratigraphic thicknesses from the region (Moore and Straub, 2001; Doelling and Willis, 2006). This construction shows that, at the onset of Laramide deformation, the burial depth of the top Navajo Sandstone was around 1220 m (non-

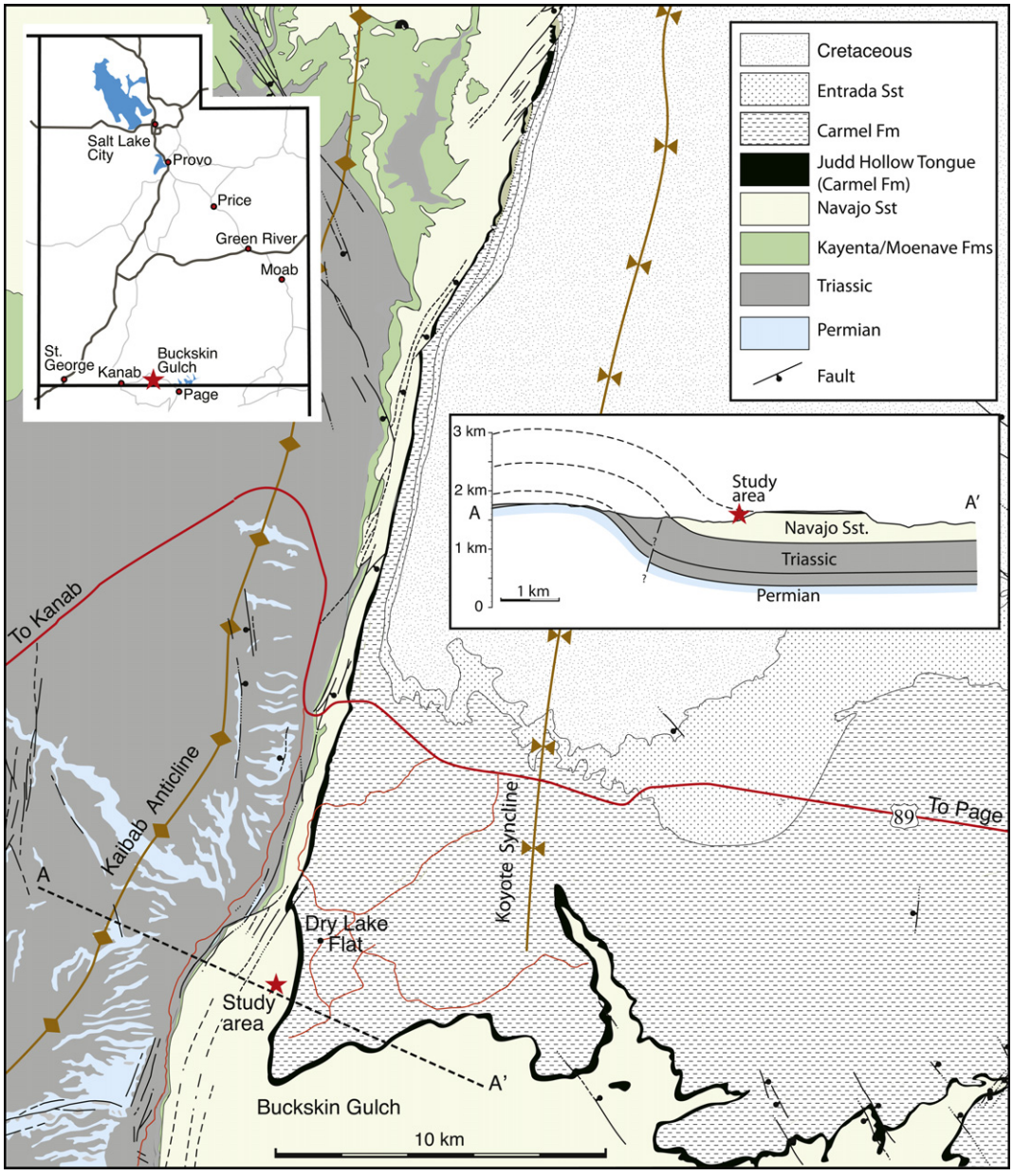

Fig. 1. Geologic map of part of the E Kaibab monocline, showing the location of the Buckskin Gulch study area.

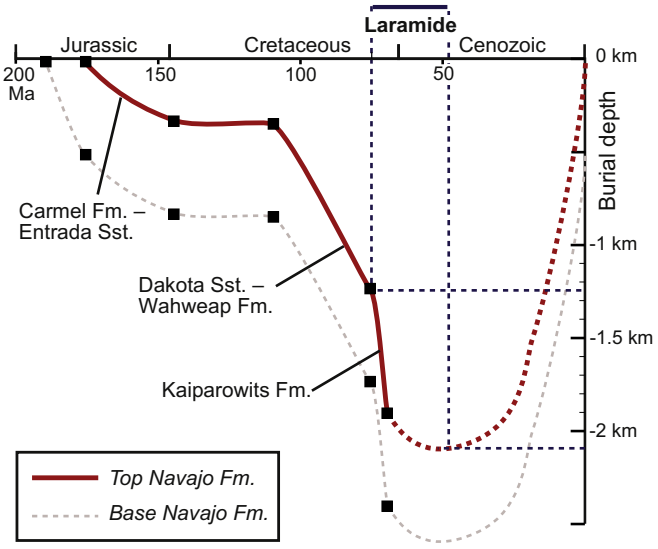

Fig. 2. Burial graph of the Navajo Sandstone (top and base) based on stratigraphic information from the East Kaibab area (not compensated for compactional effects).

decompacted section). Through the last part of the Cretaceous the fluvial Kaiparowits Formation was deposited as a response to erosion of the Sevier hinterland in southern Nevada, increasing the overburden by at least 670 m (thickness from Doelling and Willis, 2006) to a total burial depth of around 1900 m. Tertiary sedimentary strata are absent in the area, hence the burial depth during this period is not very well constrained.

2.1. The Navajo Sandstone

The Navajo Sandstone is a regionally developed Jurassic erg unit that covers most of the Colorado Plateau, reaching a thickness of around 500 m in the Buckskin Gulch area (Blakey et al., 1988). With typical porosities around 20–25%, it is the most porous sandstone unit in the Mesozoic–Cenozoic sedimentary package of the Colorado Plateau, and the only unit in which compaction bands have been found.

In the study area the Navajo Sandstone is almost entirely built up of stacked units of cross-bedded eolian sandstones. The dune units are separated by very gently E-dipping planar bounding surfaces (S_0 in Figs. 3a and 4a), and higher-order bounding surfaces locally occur within the dune units. On the microscale, the sand grains in the dune cross-strata are well rounded and, for the most part, very well sorted, consisting of predominantly quartz grains together with some feldspar and carbonate grains. Clay and iron-rich hydroxides are local cement-forming minerals, although the amount of cement is generally small. There is evidence of some dissolution at quartz grain contacts (Fig. 3c).

The characteristic grain size varies from around 0.2 to 0.5 mm within each dune unit. This variation is systematic along cross-strata and relates to the way the strata were deposited. The sand dunes are mainly composed of grain flow layers that formed as sand avalanched down the oversteepened slip face (lee side) of the dune. Grain dispersive sorting during the grain flow process caused the grain flow layers to be coarsest and best sorted, and therefore most porous and permeable, in their basal parts. Sorting becomes poorer up dip, not only because of the grain flow-related sorting process, but also because of the addition of finer-grained sand from grainfall. Grain flow layers are separated by thinner and more fine-grained grainfall layers and wind ripple laminae created by reverse winds or crosswinds between each grain flow event.

There are also significant volumes of mobilized sand that became homogenized during soft-sediment deformation shortly after burial. These homogenized sand bodies show few or no remnants of the original sedimentary structures and rarely host deformation bands. In contrast, the sandstones around the homogenized sand units show abundant evidence of soft-sediment deformation in the form of folding and multiple non-cataclastic shear bands (SB in Fig. 3b) known as disaggregation bands (e.g., Fossen, 2010a). These soft-sediment deformation bands are easily distinguished from the bands discussed in this paper by not forming positive, weather-resistant band structures (Fig. 3b, also see figure 7.41 in Fossen, 2010b, which is from the same locality). Their non-cataclastic nature has been documented from thin sections and agrees with their negative or neutral relief in outcrop.

3. Structural observations

The structures mapped in the Buckskin Gulch study area are various types of cataclastic deformation bands, i.e. bands that involve tectonic grain crushing in addition to compaction by grain reorganization (granular flow). Their positive relief due to their higher resistance to weathering makes them stand out in the field, and they consistently postdate the afore-mentioned disaggregation bands that formed by means of frictional grain sliding and rolling prior to lithification (Fossen, 2010a).

The cataclastic deformation bands in the field area all involve compaction to various degrees, and can be subdivided into three types; pure compaction bands, shear-enhanced compaction bands and compactional shear bands, some of which show internal slip surfaces (Fig. 5).

3.1. Pure (crooked) compaction bands

The pure compaction bands, called crooked compaction bands by Mollema and Antonellini (1996) and also described in Schultz et al. (2010), show a characteristic wavy or crooked geometry (Fig. 3b–d). The thickness is around 1 mm and the wavelength is typically around 0.5–2 cm (15 grain diameters in Fig. 3c), comparable to the wavelength produced in some triaxial compression tests of sandstone (e.g., Stanchits et al., 2009). They are therefore smaller than most of the chevron-style compaction bands found in Valley of Fire (e.g., Eichhubl et al., 2010), which can be considered as zigzag-style arrangements of conjugate shear-enhanced compaction bands. It is possible that this crooked geometry stems from the way compaction bands form by coalescence of pore collapse clusters (Fortin et al., 2009; Stanchits et al., 2009), although our present understanding of their formation is limited. The crooked compaction bands show no detectable shear offset of any sedimentary lamination or structures that they cross, and together with their strongly wiggly geometry, which is incompatible with shear displacement, they appear to be pure compaction bands without any involvement of shear.

In thin section these pure compaction bands show a marked, although variable, reduction in porosity that involve some grain fracture (Fig. 6) and dissolution at grain contact points (Fig 3c). Most pure compaction bands are from a few centimeters to a few decimeters in length, and are clearly restricted by lithological interfaces (Fig. 3a, b), as discussed in more detail below. The pure compaction bands occur as subvertical structures with an average strike around N010E–N015E (Fig. 4b), parallel to the general strike of the East Kaibab monocline.

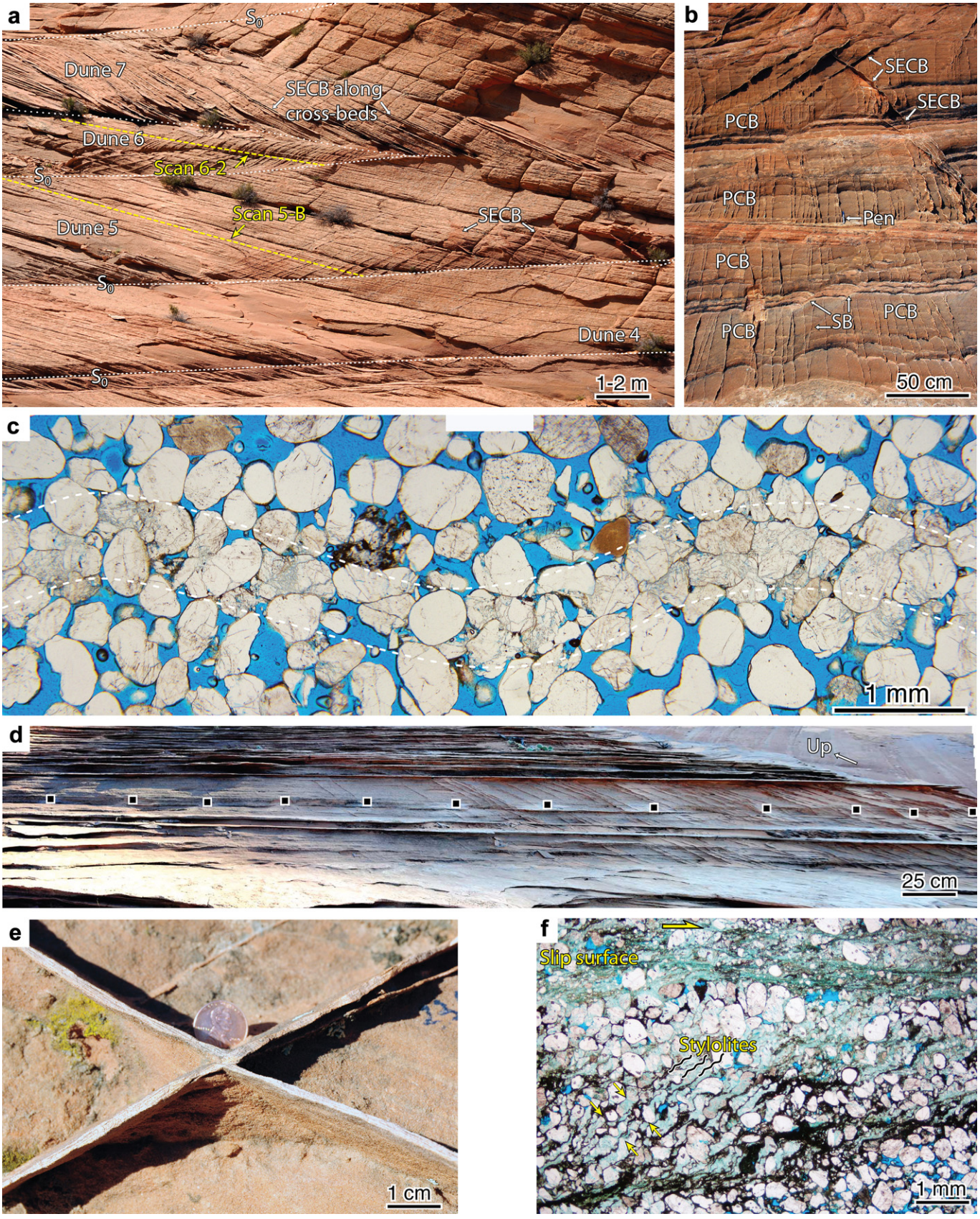

Fig. 3. a) Shear-enhanced compaction bands (SECB) localized to lower parts of dune units. PCB = Pure compaction bands. b) Occurrence of pure compaction bands in very high-porosity layers. Note conjugate sets of SECB and soft-sedimentary shear bands (SB) overprinted by pure compaction bands (CB). c) Pure compaction band (thin section). d) Variation in compaction band density along grain flow cross-strata, showing TinyPerm stations. This transect corresponds to 9-23-09b1 in Fig. 8. e) Shear-enhanced compaction bands (SECB). f) Slipped compactional shear band, slip surface in uppermost part. Shear offset is a few cm. Note pressure solution below slip surface (arrows).

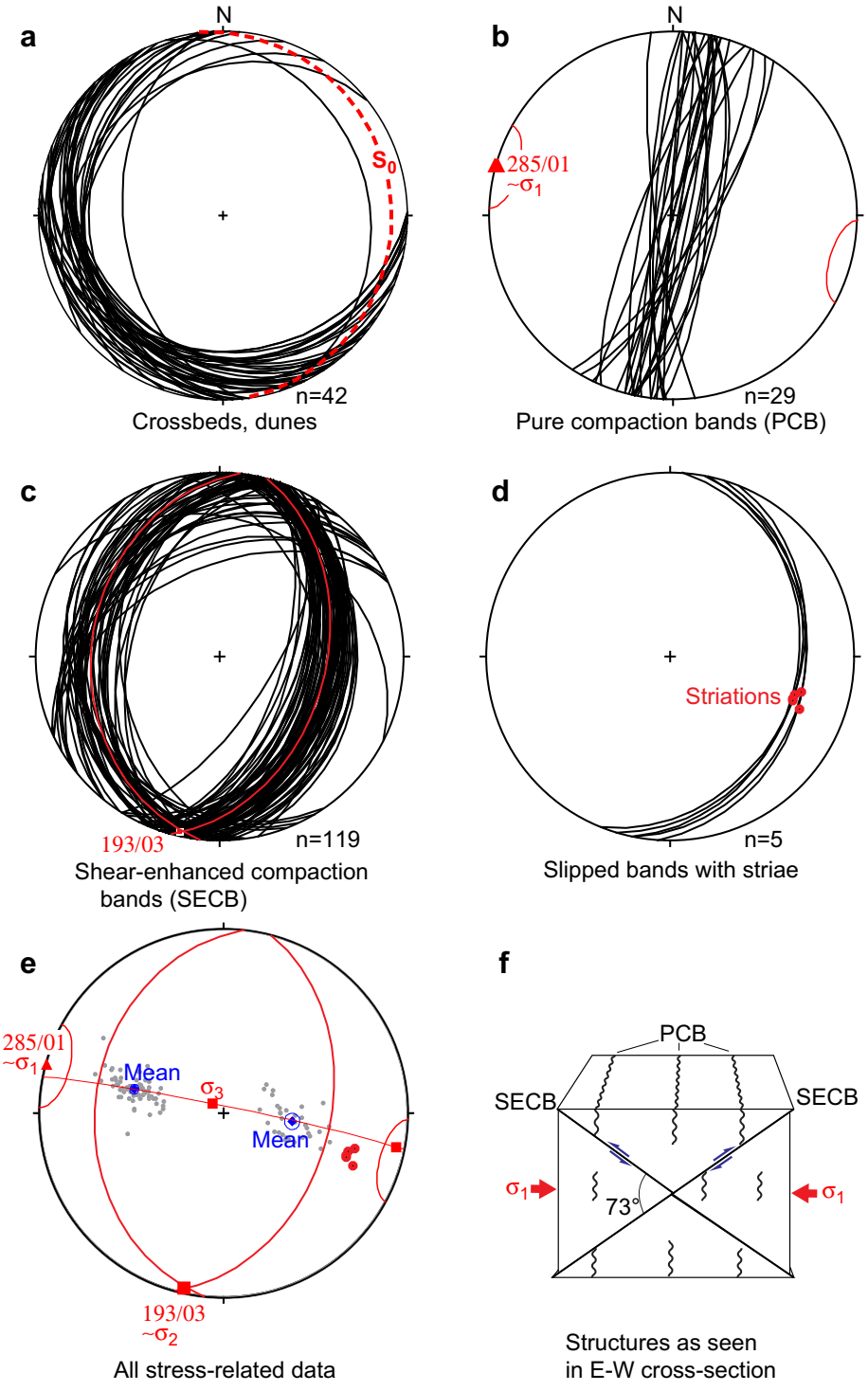

Fig. 4. Orientation data from the study area. See text for discussion.

3.2. Shear-enhanced compaction bands

Subplanar deformation bands occur as dipping structures in the study area. Many of these bands (called thick compaction bands by Mollema and Antonellini, 1996) are thicker than the pure compaction bands, ranging in thickness from two millimeters to several centimeters (Schultz, 2009). They involve significant amounts of compaction, but additional reverse shear offsets can be identified for many of them where they cross-cut laminae or each other. The shear offsets are small, rarely more than a millimeter or two (Fig. 3e) and may be difficult to detect in the field. This leaves some uncertainty as to whether all of these subplanar deformation bands actually have an associated shear component, or if some of them in fact are planar pure compaction bands. A less direct argument in favor of a small shear component on these planar compactional bands is that they commonly exhibit eye-structures where interacting tips mutually curve toward each other. Together, these observations imply that the bands have a small

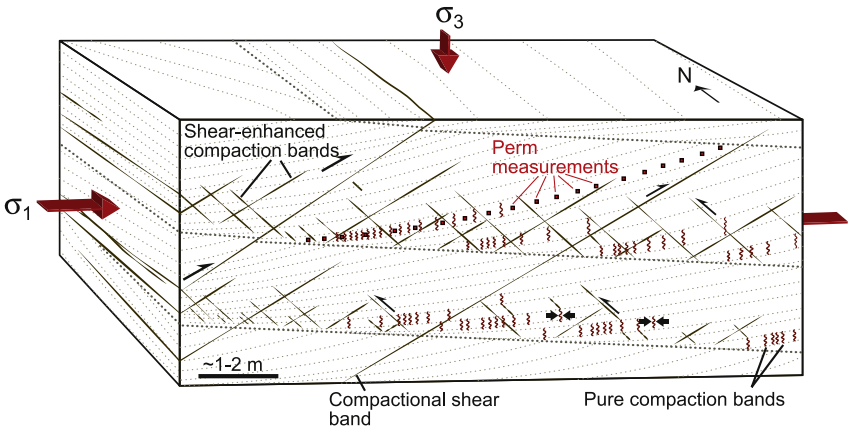

Fig. 5. Simplified sketch showing the occurrence of deformation bands in the study area and their relation to principal paleostress axes. TinyPerm data collection along a single cross-bed is indicated.

component of shear (e.g. Mollema and Antonellini, 1996), and we refer to them as shear-enhanced compaction bands in accordance with the terminology used by Eichhubl et al. (2010) for similar bands in Valley of Fire. Hence, in concert with Schultz et al. (2010) we subscribe to the very useful reinterpretation of compaction bands done by Eichhubl et al. (2010) and find close parallels between their descriptions from Valley of Fire and our study area.

Shear-enhanced compaction bands commonly form two oppositely dipping sets that mutually cross-cut each other and therefore define conjugate sets (Figs. 3b, e and 4c, f). The dihedral angle between the two sets is 73°, which is close to the 75° angle reported by Eichhubl et al. (2010) for similar sets of shear-enhanced compaction bands in Valley of Fire. This angle is higher than the commonly quoted 60° angle for shear planes, and with reference to triaxial experiments of porous sandstones (Friedman and Logan, 1973; Olsson, 2000), Eichhubl et al. (2010) made the point that this angular relationship is consistent with localization by means of shear-enhanced compaction. Microscopic investigations have shown that several of the shear-enhanced compaction bands portray more intense grain crushing than the pure compaction bands. This is also consistent with a component of shear, as laboratory experiments indicate that shear generally increases the amount of grain crushing in deformation bands (Baud et al., 2006).

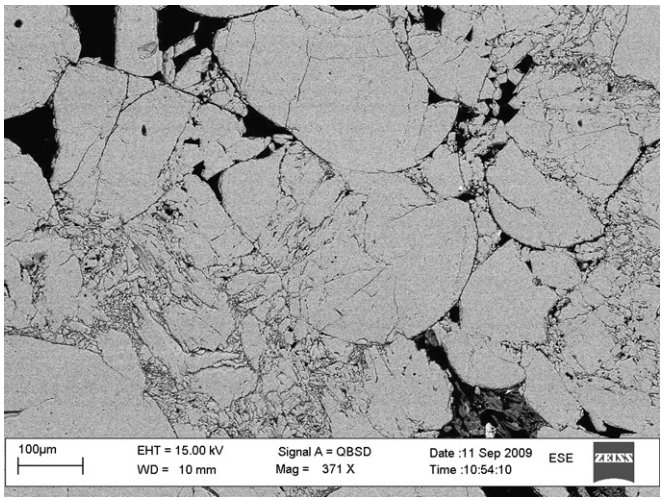

Fig. 6. Backscatter SEM image of a pure compaction band, showing clear evidence of grain breakage.

The average line of intersection between the two sets approximately parallels the strike value of the pure compaction bands (Figs. 4c and 5) and therefore is taken to represent the orientation of the principal stress axes. Shear-enhanced and pure compaction bands appear to have formed during the same progressive deformation history, because pure compaction bands locally transform into shear-enhanced bands as they enter less porous layers rather than one type of bands offsetting the other (Schultz et al., 2010). As argued below, these composite structures may have initiated as pure compaction bands that gradually expanded into adjacent lower-porous layers as shear-enhanced deformation bands as the stress level increased. This change in orientation from vertical pure compaction bands to dipping planar shear-enhanced deformation bands supports the interpretation that there is indeed a component of shear on the latter bands, even if this component may be difficult to detect in the field.

3.3. Compactional shear bands

Some of the deformation bands in Buckskin Gulch that involve shear have accumulated cm-scale shear offsets. These bands are identical to the shear-enhanced bands regarding orientation and morphology, but are longer as they extend into over- and/or underlying sandstone units. We interpret these bands as shear-enhanced bands that have accumulated additional shear offset during the course of deformation. Hence, the development of deformation bands in these rocks seems to go through an early dominance of shear-enhanced compaction and then, when porosity has been reduced so that compaction becomes more difficult, deformation approaches simple shear. Further to this development, some of the compactional shear bands have developed an internal striated slip surface with less cohesion than the rest of the band. This indicates a late-stage (high-strain) localization of the shear, quite similar to slipped normal-sense deformation bands described from the Nubian Sandstone in Sinai (Rotevatn et al., 2008). The slip surfaces, which in Buckskin Gulch show reverse sense of slip, may be discontinuous (patchy), and thin section studies show that they are thin (<0.5 mm) ultracataclastic zones associated with zones of well-developed pressure solution surfaces oriented ~45° to the slip plane (Fig. 3f). This orientation indicates that at this advanced stage compaction is completed, and strain accumulates by approximately isochoric simple shearing. These deformation bands show cm-scale shear offsets and are more extensive than the shear-enhanced compaction bands (Fig. 5). These bands may occur as single structures, but also in deformation band shear zones of the type described by Davis (1999).

4. Stress field

Numerous experiments show that pure compaction bands form perpendicular to the local maximum shortening direction (e.g., Tembe et al., 2008), which for the small strains involved can be taken to approximate the maximum principal stress (σ_1) direction. Field measurements show that the pure compaction bands are subvertical structures striking around N013E or S193W, indicating that $\sigma_H = \sigma_1$ is close to 285/01 (Fig. 4b).

The orientations of the conjugate shear-enhanced compaction bands can also be used to constrain σ_1. Most of these bands conform to an orientation pattern where σ_1 bisects the obtuse angle of the bands ($\sim 73^\circ$). This approach gives an orientation of σ_1 at 101/06 and a subvertical σ_3, i.e. very close to the previous estimate. Slip directions on slipped compactional shear bands with reverse offsets (Fig. 3e) are consistent with these estimates. The paleostress data are summarized in Fig. 4e.

5. Permeability, porosity and frequency measurements

5.1. Methods

Porosity has been estimated from thin section images obtained from both host rock and from deformation bands. Optical images have been used for host rock porosity estimates, while SEM backscatter images were used to estimate porosity within deformation bands. Independently, routine ambient-porosity laboratory measurements have been conducted on plugs collected in the field.

Permeability has been measured in three independent ways: 1) in situ measurements by means of the TinyPerm II portable hand-held air permeameter, 2) by image analysis, and 3) by routine gas-based laboratory plug measurements.

In situ permeability measurements, hereafter referred to as TinyPerm data, were performed on dry outcrops with the TinyPerm II portable hand-held air permeameter, manufactured by New England Research (NER). TinyPerm measurements were carefully collected across dry, fresh and planar rock surface free of dust and without any weathering effects. 3–5 measurements were taken at each point to sort out anomalous measurements. The advantage of this non-destructible method is rapid and reproducible results and an opportunity to measure even the most friable high-porosity sandstones that were impossible to drill for laboratory measurements and difficult to sample for thin section preparation. In this way, permeability variations across dunes and, in particular, along dune cross-strata with deformation bands concentrated to their lower parts, were mapped.

Plugs from the parts of the sandstones that were cohesive enough for drilling were subjected to laboratory gas (Helium) measurements of permeability (performed by TerraTek, Salt Lake City). Permeability of these plug samples was also determined for optical and SEM backscatter thin section images using the method described in Torabi et al. (2008).

Deformation band frequency data were collected along scanlines across stratigraphic units and along cross-beds within sand dune units. Frequency, permeability and porosity data were collected from the same scanlines for direct correlation.

5.2. Permeability versus band frequency

Field observations in the study area revealed that shear-enhanced compaction bands and, particularly, pure compaction bands, are concentrated in the lower parts of the sand dune beds (Fig. 3a). This characteristic occurrence of deformation bands was quantified by making deformation band maps or frequency recordings across dune units (Fig. 7), coupled with TinyPerm permeability analyses of undeformed sandstone between or away from deformation structures.

It is clear from such observations that shear-enhanced compaction bands occur more frequently where permeability (and therefore porosity) is high. It is also clear that deformation bands with unambiguous shear offsets have propagated through several dune units with no apparent dependence of porosity variations within the range represented by these dune deposits. Fig. 7 (at 4–5 m in Dune 9-22-09i) shows how such bands locally start developing into deformation band shear zones.

Detailed studies of the relationship between deformation band frequency and permeability were done *along* selected eolian cross-strata (see Figs. 3a, 3d and 5), since every dune unit is composed of cross-strata that show gradual bedding-parallel variations in grain size, sorting and porosity. The results (Fig. 8) show a very close relationship between deformation band frequency and permeability, where the maximum permeability and band density is found shortly above the base of each dune layer, tapering off toward the top of the dune unit.

This pattern is seen for shear-enhanced compaction bands (Fig. 8a–c), and these bands preferentially occur in sandstones of TinyPerm permeability in excess of ~0.5 darcy (Fig. 9a). A much more systematic relationship is found for pure compaction bands (Fig. 8d–f). These bands only occur in the most permeable parts of the dunes, and the data show that a linear relationship exists between compaction band frequency and permeability in these locations (Fig. 9b). The lower cut-off value for the data set is a TinyPerm permeability of around 18 darcy, with an uncertainty represented by the range shown in Fig. 9b (6–32 darcy).

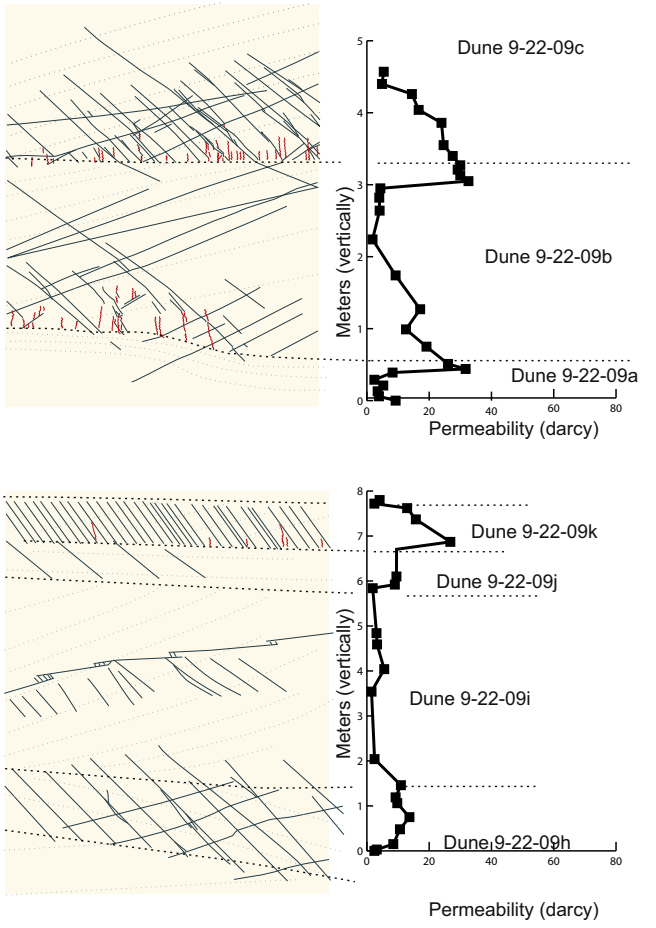

Fig. 7. Permeability across dune units, showing how deformation bands preferentially occupy highly permeable parts of the sandstones.

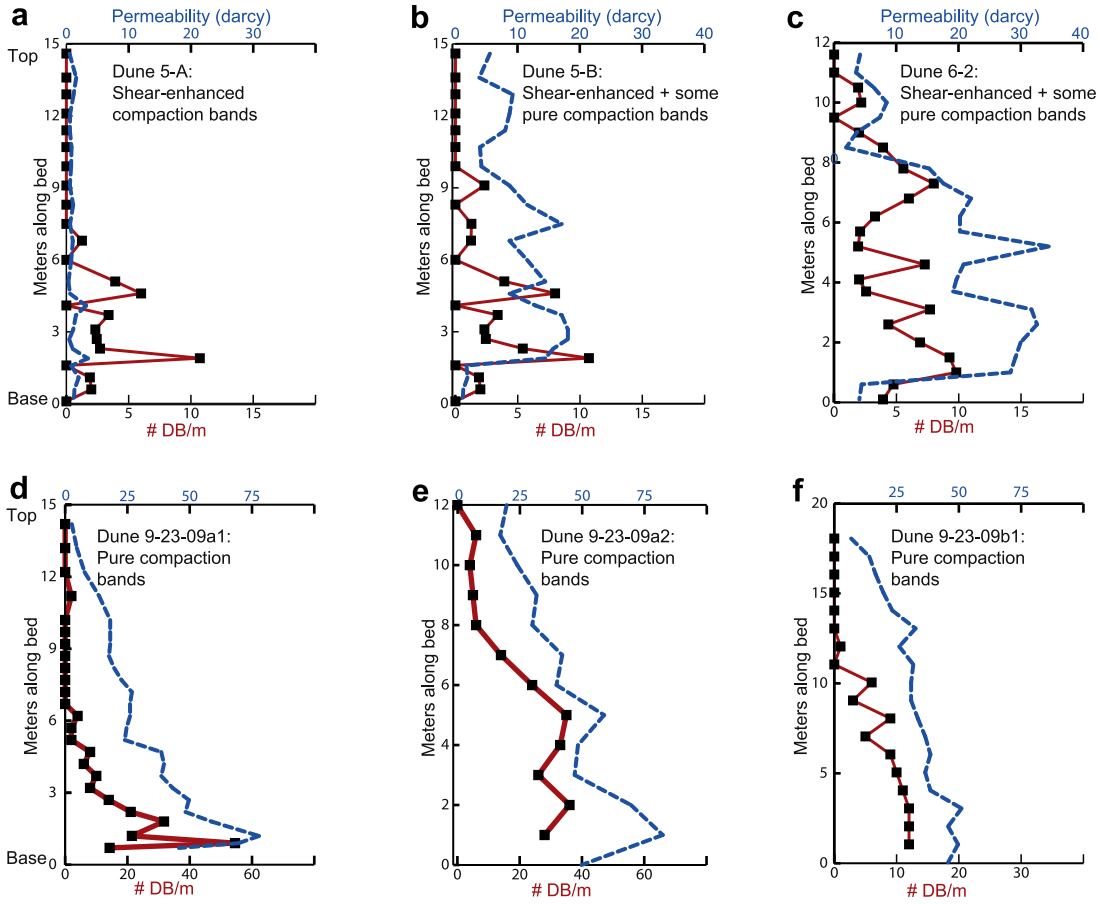

Fig. 8. Paired profiles recording band density and permeability along cross-strata in individual dune units.

5.3. *Comparing and calibrating permeability*

Permeability can be estimated in several ways, notably by means of standard plug evaluations (gas permeability), image analyses, and in situ (TinyPerm) permeability as reported above. These different methods provide us with different measures of permeability that are likely to differ to some extent. In particular, TinyPerm values are estimated based on a calibration function that is provided by the manufacturer (New England Research), and this general calibration function may not be optimal for the eolian sandstones explored in this study.

The gas plug permeability method, where the effective permeability is measured along an inch-long plug, is a standard method within the petroleum industry, so to compare plug data with our TinyPerm values we drilled plugs at some of the TinyPerm stations. Because of the difficulties obtaining plugs from the most porous and friable sandstones, the range is limited, but the results give a positive correlation where the TinyPerm is ~1.8 times the

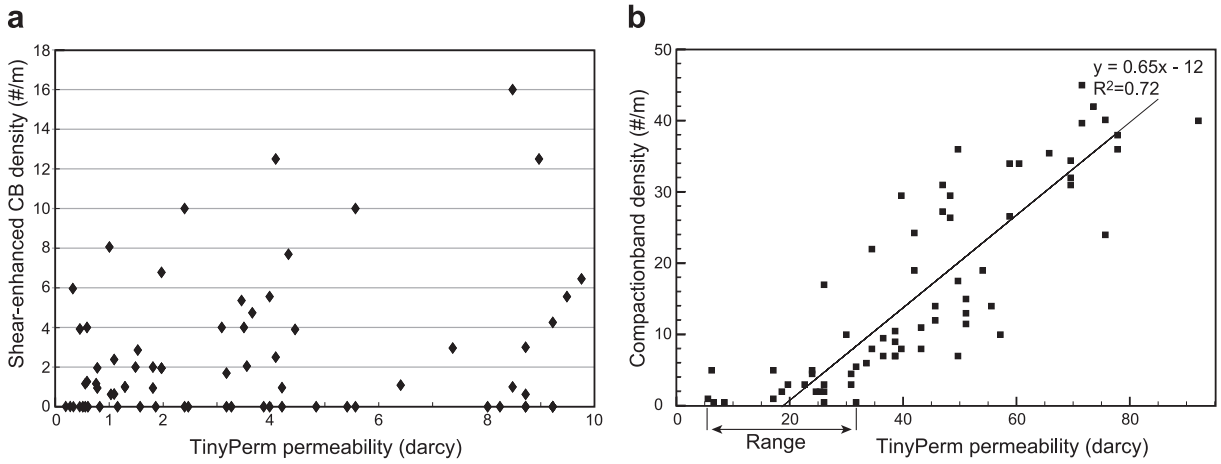

Fig. 9. a) Relationship between density of shear-enhanced compaction bands and TimyPerm permeability, showing that SECBs occur in sandstones with permeability greater than ~0.3 darcy. b) The same plot for pure compaction bands, showing a positive trend between permeability and band density with a best fit line intercepting the horizontal axis at 18 darcy, corresponding to ~10 darcy for plug measurement (see Fig. 10a).

standard plug permeability values. Including data from Jurassic dune deposits from other locations in southern Utah confirms a correlation factor of 1.8 (Fig. 10a). Using this correlation, it is found that pure compaction bands only form in the eolian sandstones where plug permeability exceeds an average value of 10 ± 7 darcy.

As a second control we have extracted permeability from image analyses of thin section images (optical and SEM) from the same plugs. Details about this image-based method can be found in Torabi et al. (2008). Comparing plug and image data from the present study suggests that the TinyPerm values overestimate the image-based permeability values by a factor of ~1.7 (Fig. 10b), i.e. a correlation that compares well with the plug permeability versus TinyPerm correlation described above.

5.4. Calibrating porosity

Porosity was estimated from plug tests and from image analyses, and correlated with permeability. Fig. 10c shows the correlation between plug permeability and plug porosity. Because of the difficulties of collecting plugs from the most porous parts of the sandstones, the range is limited, and the slope is poorly constrained. Image porosity–permeability data show a wider scatter (Fig. 10d), because this approach is sensitive to small-scale heterogeneities. However, the range in data is larger so that the correlation between image permeability and image porosity is established for a wider range of values. Using these data we can convert the ~10 darcy statistical cut-off permeability value to around 29% porosity, meaning that compaction bands only form in these sandstones where the porosity exceeds ~29%. Considering the uncertainty range shown in Fig. 9b, the critical porosity value for the studied deposits should fall between 25.6 and 32.4% (i.e., $29 \pm 3\%$). A single exact number cannot be found because of the natural variations in porosity and permeability even at cm-scale in natural sandstones, but the range gives a clear indication that very high permeability and porosity values are required in these rocks for compaction bands to form.

5.5. Porosity and permeability within deformation bands

All types of deformation bands in the Buckskin Gulch area have a negative effect on porosity and permeability. Image analyses show that the porosity is decreased by 0–4 orders of magnitude as compared to the immediately surrounding host rock (Fig. 11). Similarly, the porosity reduction varies from almost none to 10% of the original porosity, with the greatest reduction recorded being from 35% in the host rock to 4% in the band. These great variations in porosity reduction reflect variations in amount of cataclasis and dissolution within the bands, which can be seen from Fig. 6 to occur at the millimeter scale. In general, these values fall within the typical range of porosity and permeability reductions for deformation bands (e.g. Fossen and Bale, 2007).

6. State of stress

The yield envelope in the q–p diagram marks the range of stress states at which strain in a given sand or sandstone transitions from elastic to inelastic (e.g., Aydin et al., 2006; Okubo and Schultz, 2007; Wibberley et al., 2007; Saillet and Wibberley, 2010; Schultz et al.,

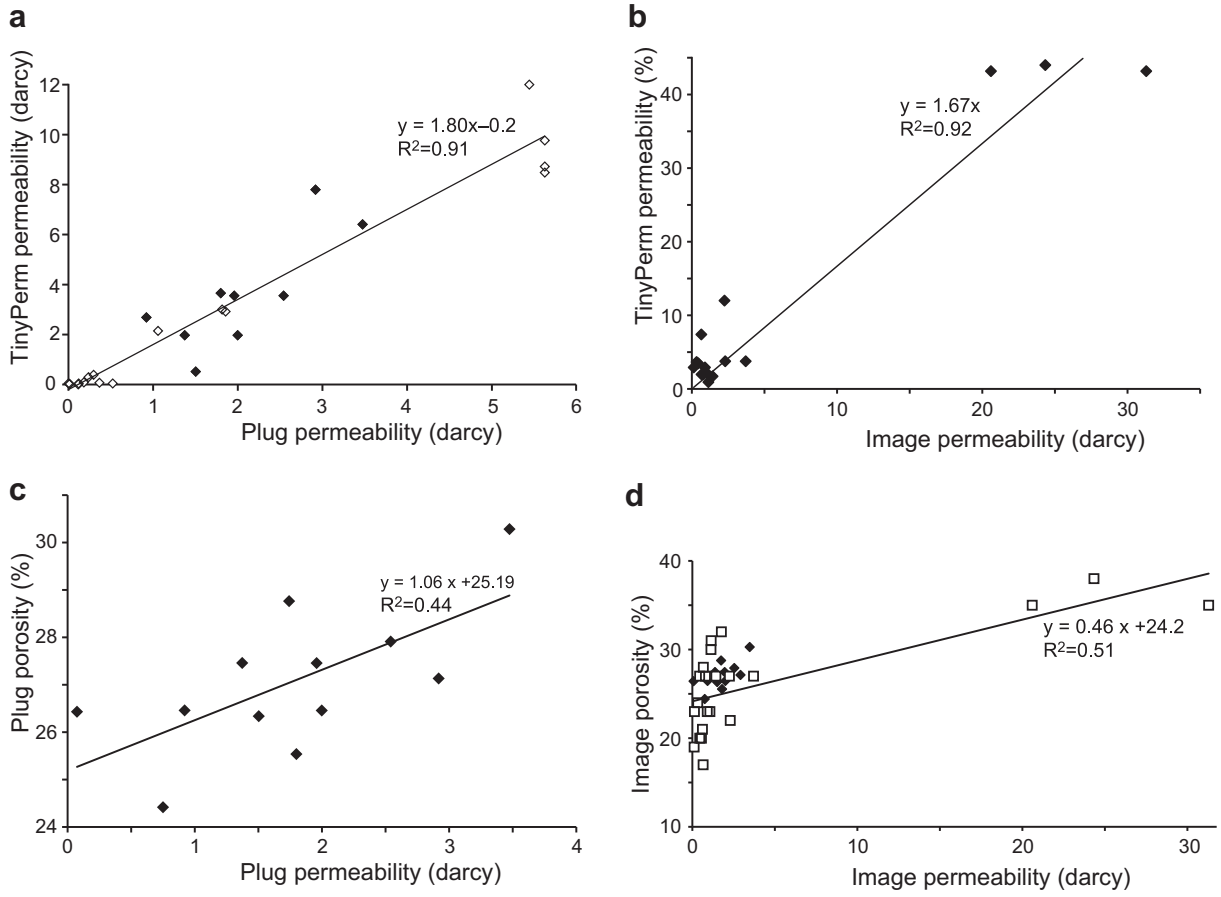

Fig. 10. Graphical representation of the relationship between (a) TinyPerm and plug permeability, (b) Tinyperm and image-based permeability, (c) porosity and permeability from plug measurements, and (d) image-based porosity and permeability. In (d) we also show the plug data from (c) for comparison.

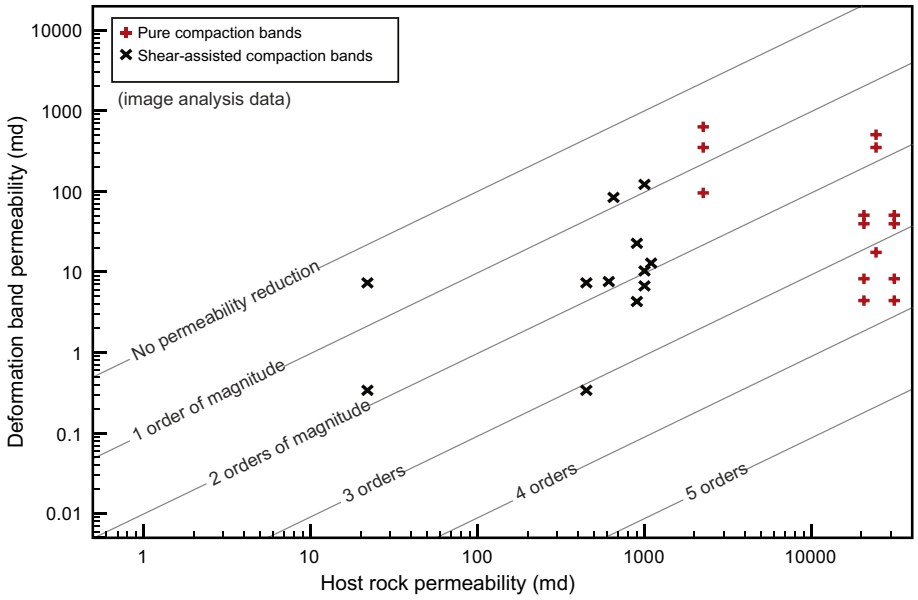

Fig. 11. Permeability of deformation bands in relation to surrounding undeformed (host) rock, as estimated from image analyses.

2010). In this diagram, where the horizontal axis q represents differential stress $(\sigma_1 - \sigma_3)$ and p is the mean effective stress $((\sigma_1 - \sigma_2 - \sigma_3)/3)$ (Fig. 12), the yield surface depends on the strength of the sand(stone), and moves to the right during lithification. Numerous experiments (e.g., Zhang et al., 1990; Wong et al., 1997) have mapped the yield envelope for various stress conditions, showing that the envelope is, to a first approximation, elliptical, especially on the cap side of interest to this study.

The right-hand (cap) side of the yield envelope is of particular interest, because it describes the stress conditions causing compactional deformation. Ideally, pure compaction (uniaxial contraction) occurs when q is relatively close to 0, so that pure compaction bands form where the yield envelope approaches the p-axis with small or moderate differential stress q. In our field example the state of stress is not on the p-axis, because the consistent preferred orientation of the pure compaction bands reflects a significant difference between σ_1 and σ_2.

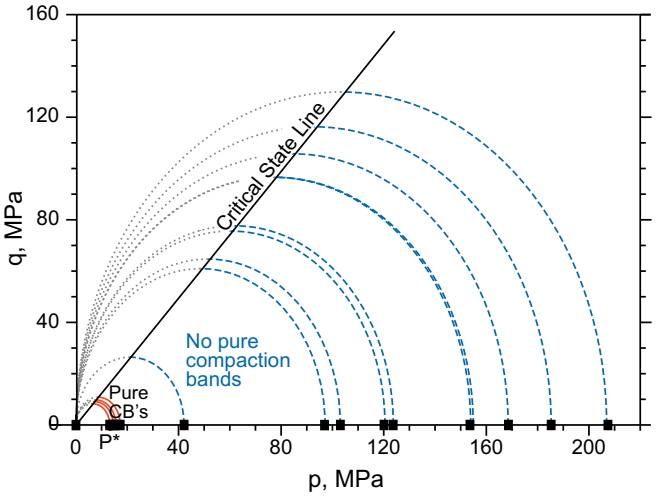

Fig. 12. q–p diagram showing caps for various lithologies in the Navajo Sandstone in the field area. Calculated critical p-values (P^*) for layers containing compaction bands are around 10–20 MPa. q is differential stress, and p is the mean stress.

Experimental work (Zhang et al., 1990) has shown that for sand(stone), a critical mean effective stress (also called grain crushing pressure) P^* (in MPa) depends on porosity n (expressed as a fraction) and grain size R (in mm) through the equation $P^* = (nR)^{-1.5}$. Using this equation, P^* associated with grain cracking can be estimated for the various parts of the Navajo Sandstone, and the value depends on the local grain size and porosity. This exercise has recently been done by Schultz et al. (2010) for 5 layers in the Buckskin Gulch area, who estimated that compaction bands form at $P^* \approx 22$ MPa. We here follow the same approach, add more data and correct the data for the sectional effect associated with porosity estimates from thin section.

We have estimated P^* using porosity and average grain size estimates from dyed thin sections from lithologies with and without pure compaction bands. The grain size from thin section measurements were multiplied by a factor of 1.273 to compensate for the 2D effect associated with thin sections (see Kong et al., 2005). The results (Fig. 12) indicate that the pure compaction bands form where P^* was less than 20–40 MPa, which is in close agreement with estimates made by Eichhubl et al. (2010) and Schultz et al. (2010). At $P^* \geq 40$ MPa, shear-enhanced deformation bands formed without the formation of pure compaction bands. For the highest porosities and coarsest samples studied here, P^* is as low as ~15 MPa. This indicates that, as stress increased in these rocks, the first pure compaction bands formed in the most porous and coarse-grained layers at around 15 MPa, corresponding to a depth of ~1 km (assuming lithostatic stress, hydrostatic fluid pressure and a dry rock density of 2450 kg/m^3).

7. Discussion and conclusions

7.1. Timing and stress field

The conjugate sets of shear-enhanced compaction bands define an isotropic stress field where σ_1 is N100E and perpendicular to the pure compaction bands. Since all of these bands are consistent with such a stress orientation, we take this as evidence that the pure compaction bands in the Buckskin Gulch area formed perpendicular to σ_1. This stress field orientation agrees with the formation of the East Kaibab monocline as a reverse fault-

propagation fold (Schultz, 2011) and with the Laramide deformation of the Colorado Plateau in general. Mollema and Antonellini (1996) suggested that some of the pure compaction bands formed in the compressive quadrant of small faults, but the distribution of compaction bands (e.g., Fig. 3d) and their clear dependence on lithologic parameters (Fig. 8) documented here do not suggest that this model has general applications in the Buckskin Gulch area.

Although all of the deformation bands that we have observed appear to have formed during the same regional stress field or deformation phase, we speculate that pure compaction bands were the first to initiate because, according to grain size- and porosity-based stress calculations above, they do so in the most porous sandstones under estimated mean stresses as low as 10–20 MPa. This stress level corresponds to ~1 km of burial depth, and although this depth estimate is not very accurate, it may suggest that pure compaction bands initiated at an early stage of the Laramide phase, prior to or at an early stage of deposition of the Kaiparowits Formation (Fig. 2). Shear-enhanced compaction bands started to form at a higher stress level as tectonic stress increased during the Laramide phase (principal stresses having a constant orientation throughout this development). At late stages of this development the compactional shear deformation bands with slip surfaces and deformation band shear zones formed. This simple model of deformation band development is shown schematically in Fig. 13.

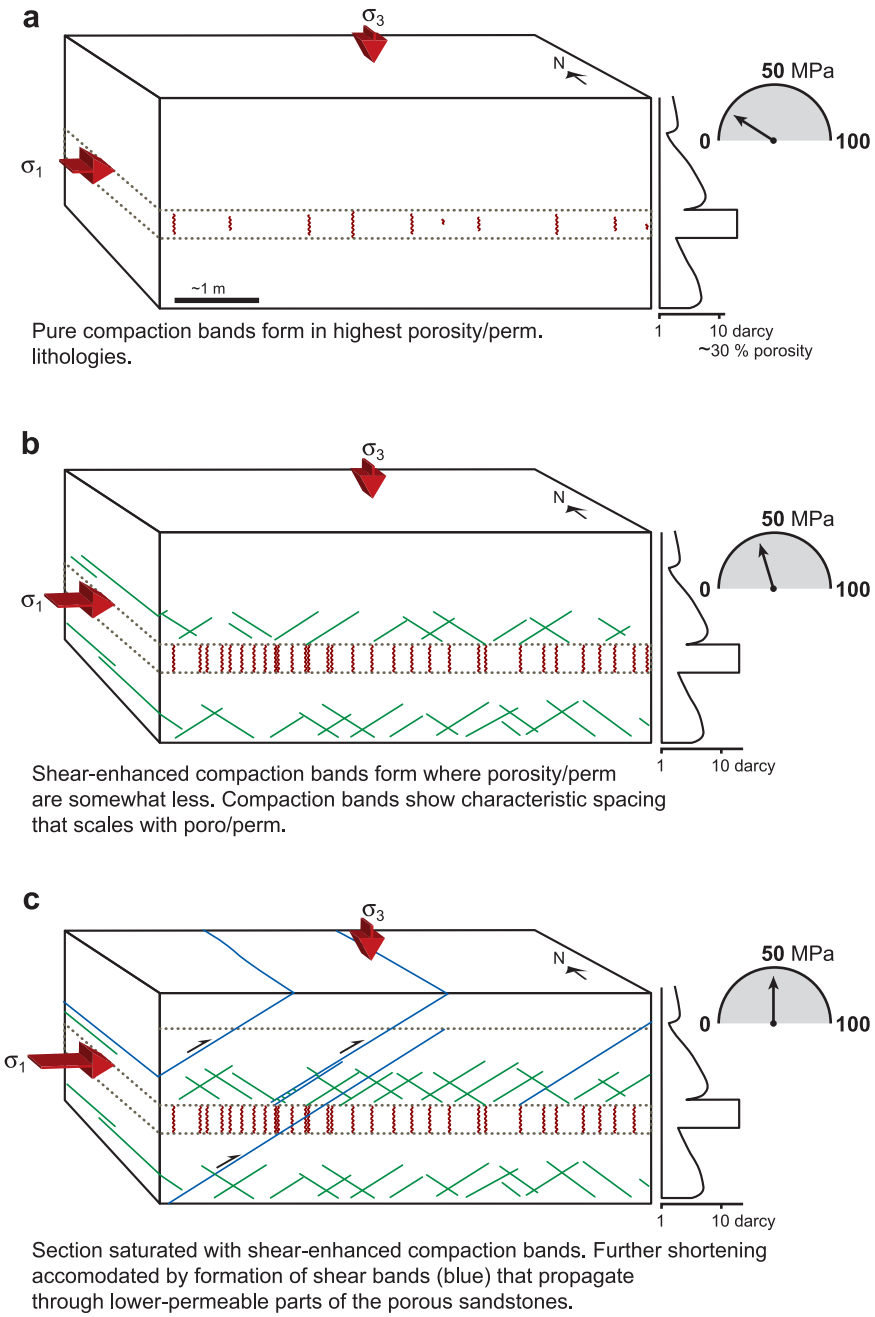

Fig. 13. Schematic illustration of the evolutionary history of deformation bands in the study area. The dependence of band formation and growth on petrophysical parameters (permeability and grain size) is indicated together with the critical mean stress at various stages. A mean stress meter is shown on the right.

7.2. Premises for compaction band formation

A number of variables influence the formation of deformation bands in general, and compaction bands in particular. These include grain size, shape, mineralogy, cementation, porosity and the distribution of heterogeneities in the sandstone. Porosity is probably the most important of these, and for the sandstones studied at Buckskin Gulch, pure compaction localization structures only formed where porosity $> 29 \pm 3\%$ and permeability $> 10 \pm 7$ darcy. Note that these numbers are minimum estimates, since burial after compaction band formation must have reduced porosity by an unknown extent. At the same time several studies indicate that some cementation at grain boundaries is needed for cataclastic compaction bands to form, or more specifically to allow stress across grain contacts to exceed the critical tensile strength of the grains (e.g. Haimson and Lee, 2004; Aydin et al., 2006; Marketos and Bolton, 2009). This may suggest that the cataclastic compaction bands that we observe formed under conditions that favorably balanced bond strength and porosity, i.e. very high porosity but where grain contacts have sufficient strength (just enough cementation) to promote grain breakage. More experimental work is needed to investigate this relationship further.

In layers with somewhat lower porosity ($<29 \pm 3\%$), compaction is assisted by shear to form shear-enhanced compaction bands, and the bands are oriented oblique to σ_1, generally in conjugate sets bisected by σ_1. We see an evolution from short bands with practically invisible amounts of shear to longer bands with cm-scale shear offset, suggesting that compaction must be important in the early stages of the history of such bands, while shearing becomes more important when porosity has been reduced within the band. Furthermore, the fact that only bands that have accumulated cm-scale shear offsets transect complete dune units tells us that shearing eases cross-stratigraphic band propagation.

Factors such as mineralogy, grain size, grain shape and grain crushing strength may influence the quantitative aspects of these results. Since the compaction bands studied here (and in experiments) involve cataclasis, the grain crushing strength puts a minimum stress value limit on the formation of compaction bands. An increase in feldspar or lithic content is likely to lower the strength of the sandstone, causing the sample to yield at lower stress levels and/or lower porosity values. Drilling experiments by Haimson and Lee (2004) give some indications that compaction localization occurs more easily in sandstones with high (>90%) quartz content. Tembe et al. (2008), on the other hand, produce compaction bands in Diemelstadt Sandstone with a feldspar content of 26%, so the role of mineralogy is not clear.

Grain shape and sorting in part connect to porosity, and the suggestion made by Vardoulakis and Sulem (1995) and Antonellini and Aydin (1995) that uniform grain size and pore sizes promote the formation of compaction bands seems likely based on the present observations. Cementation and dissolution are other factors whose effects are not well understood. There is thus a great need for well-designed laboratory experiments to increase our understanding of these factors with regard to compaction localization in sandstone (Holcomb et al., 2007). Hence, we do not know how directly the results presented in this work from quartz sandstones with well-rounded and well-sorted grains, can be applied to other porous rocks or media.

In addition to stress magnitude, the state of stress may also be important. Theoretical and experimental work indicates that axisymmetric compression ($\sigma_1 > \sigma_2 \approx \sigma_3$) favors compaction localization over shear localization (Issen and Rudnicki, 2000; Olsson, 1999, 2000). Eichhubl et al. (2010) speculated that the state of stress within the rock may change over short (cm-scale) distances to the extent that it controls whether the bands will involve shear or just compaction. At Buckskin Gulch, the most porous layers yield first, thus loading the unyielded adjacent layers and thereby changing the stress state as compaction localization proceeds. Layers with pure compaction bands may then stiffen, expanding the yield cap (e.g., Grueschow and Rudnicki, 2005) to a point where it may approach those of the adjacent layers in strength, facilitating the growth of throughgoing bands.

It is important to realize that post-deformational diagenetic and compactional changes alter the porosity and permeability of the host rock, possibly obscuring the quantitative relations of compaction band formation with porosity and other characteristics of the sandstone in question. The two most important porosity and permeability-changing factors are cementation and chemical compaction in the form of quartz dissolution at grain contact surfaces (see Taylor et al., 2010 for a review of diagenetic effects). They both become increasingly important with increasing temperature and burial depth, so a sandstone that has been buried to ~3 km or more may have experienced a reduction in porosity and permeability to values far smaller than those required for compaction band formation. Hence, when predicting the occurrence of compaction bands in subsurface sandstone reservoirs, post-deformational reductions in permeability and porosity must be taken into account. In the Buckskin Gulch case deformation occurred at 1–2 km depth without post-deformational burial to much more than 2 km depth (Fig. 2). Conditions at this depth were not right for quartz dissolution to operate at significant rates. These processes are largely temperature controlled, requiring temperatures in excess of ~90 °C (Bjørkum et al., 1998). Hence some post-deformational reduction in porosity is expected for the Buckskin Gulch site, but probably not very much. It should be noted that other minerals, such as carbonate, clays and iron (hydr) oxides are mobile at lower temperatures and burial depths and thus have the potential to reduce porosity at relatively low burial depths. In the study area, iron (hydr)oxides mainly occur as very thin coatings that do not significantly affect porosity and permeability.

7.3. Comparison with other compaction bands

The compaction bands described in this work are of two types; planar and crooked, where the planar type is interpreted to involve a subordinate component of simple shear, while the crooked type involve pure compaction. Very similar sets of bands are found in the Valley of Fire area (Eichhubl et al., 2010), where the shear-enhanced compaction bands show many similarities to those in Buckskin Gulch. However, the pure compaction bands are different in detail in that they show more angular zigzag or chevron patterns with variable, but generally larger (1–15 cm) wavelengths. Their straight limbs give the impression that a shear component of opposite shear sense may be present on each limb, and one of the limbs may locally continue as a straight shear-enhanced deformation band. The reason why pure compaction bands in the Buckskin Gulch and the Valley of Fire differ in terms of wavelength, amplitude and geometry is not clear. It could relate to the distribution of mechanical heterogeneities in the sandstone, including grain flaws and pore structure, to the state of stress and stress history, or to deformation mechanisms at the grain scale level. As for the latter point, chevron-type compaction bands in Valley of Fire show less cataclasis than do the crooked compaction bands at Buckskin Gulch.

Another difference between the two areas is the somewhat lower porosities (estimated to 25% by Sternlof et al., 2005, and 22.7% by Eichhubl et al., 2010) and larger range of permeability values (TinyPerm estimates of 2–20 darcy, unpublished

observations) recorded for the host rock that contains pure compaction bands (chevron-type) in Valley of Fire than for the Buckskin Gulch site. One possibility is that the Aztec Sandstone in Valley of Fire experienced more porosity loss *after* the compaction bands formed. The Valley of Fire bands probably formed at shallower (750 m) depths than those in Buckskin Gulch, and with post-deformational burial to almost 2 km and subsequent uplift (Eichhubl et al., 2010) this opens for a somewhat more significant porosity and permeability reduction after compaction band formation.

It may be worth noting that well-defined compaction bands are only reported from experimental deformation of well-cemented sandstones with porosities typically ranging from 15 to 25%, and that confining pressures of hundreds of MPa, corresponding to crustal depths around 10 km, are required for compaction bands to form in the laboratory (e.g., Baud et al., 2006). Not only are rock properties, fluid pressure and stress conditions far removed from those relating to compaction band formation in the poorly cemented and relatively shallowly buried Navajo (and Aztec) Sandstone (Schultz, 2009), but no natural sandstone would preserve any significant amount of porosity at such crustal depths. As argued by Sternlof et al. (2005), compaction bands formed in undrained laboratory experiments, which also tend to produce more intense cataclasis, should perhaps be considered as a different type of compaction bands that initiate and propagate differently than the natural examples. The unrealistically high stress levels required to form compaction bands in well-cemented sandstones such as the Berea suggest to us that natural compaction bands are not to be expected in such lithologies. Hence there is a call for well-designed triaxial experiments conducted on weak (poorly cemented) sandstones of very high porosities.

7.4. Effect on fluid flow

In general, deformation bands retard fluid flow to an extent that depends on their permeability reducing properties, frequency and thickness. In addition, their orientations and spatial distribution in a heterogeneous sandstone unit may influence the flow pattern during injection or production of fluids. This study has shown how the distribution of deformation bands depends on local rock properties, here quantified in terms of porosity and permeability. Interestingly, the distribution pattern may have a positive effect on sweep efficiency inasmuch as it prevents fluids from selectively sweeping the extremely high-permeable layers. This effect will be greatest perpendicular to the bands, which will make macro-permeability anisotropic with a minimum effective permeability parallel to the bands. We have demonstrated how the orientations of the various types of deformation bands depend on the orientation of σ_1, hence the permeability anisotropy they impose on a reservoir can be predicted when the orientation of σ_1 at the time of deformation is known. For the present case with a single phase of deformation, our findings suggest that the permeability is going to be smallest parallel to σ_1 (E–W direction) with little permeability reduction perpendicular to σ_1 (N–S direction).

8. Conclusions

Cataclastic deformation bands in the quartz-arenitic Navajo Sandstone in the Buckskin Gulch embrace pure compaction bands, shear-enhanced compaction bands and compactional shear bands, the latter category locally with a thin ultracataclastic slip surface. Pure compaction bands only occur in layers where permeability exceeds several (10 ± 7) darcy and porosity exceeds 29 ± 3%. In such high-porosity layers, the frequency of pure compaction bands is found to increase with an increase in host rock porosity and permeability. We expect this to be a generally valid observation, but quantitatively the critical permeability, porosity and stress state needed for compaction band formation will depend on lithologic/mechanical characteristics such as grain strength (mineralogy), grain bond strength (cementation and dissolution controlled), grain sorting and grain shape.

Adding shear to compaction lowers the critical minimum porosity for deformation band formation and propagation, hence shear-enhanced compaction bands are common where porosity and permeability are too low for pure compaction bands. Furthermore, compactional shear bands, in which shear displacement dominates over compaction, can propagate into and locally through beds that are void of both shear-enhanced and pure compaction bands.

The geometric configuration of the various classes of deformation bands is altogether consistent with a single reverse- or thrust-fault stress regime with a subhorizontal σ_1 trending approximately N100E, i.e. perpendicular to the East Kaibab Monocline. The observation that the crocked pure compaction bands bisect conjugate shear-enhanced compaction bands is taken as evidence that they formed perpendicular to the regional σ_1 direction of an anisotropic (non-lithostatic) stress field. Hence, contrary to some previous workers (Mollema and Antonellini, 1996; Schultz, 2009) we do not in general interpret the planar and thicker deformation bands in the area as pure compaction bands, but rather as shear-enhanced compaction bands formed at an oblique angle to the regional orientation of σ_1. Furthermore, the relationship between faults and pure compaction bands suggested by Mollema and Antonellini (1996), where pure compaction bands form in the compressive quadrant of small faults, is not required.

Calculations indicate that pure compaction bands form at lower mean stress levels than bands involving shear, which may indicate that compaction bands were the first bands to form during the contractional Laramide deformation history of the area. Interestingly, the estimated stress conditions are considerably lower than those needed to form well-defined compaction bands in the laboratory.

Both pure and shear-enhanced compaction bands show permeability reductions by up to 3–4 orders of magnitude, but they also show significant lateral and vertical variations in permeability. In a hydrocarbon production setting these bands will reduce the effective permeability in the most permeable parts of the sandstone reservoir. The likely consequence of such a homogenization of the reservoir properties is to enhance sweep. The relationship between permeability/porosity and band frequency identified in this work can be used to predict the distribution of deformation bands in a quartz-sandstone reservoir based on available petrophysical data from the reservoir, provided that post-deformational compaction and cementation can be accounted for.

Acknowledgments

This work was conducted within the COPS (Contractional deformation Of Porous Sandstones) and the IMPACT CO_2 projects at Center for Integrated Petroleum Research (CIPR), and by NASA's Planetary Geology and Geophysics Program (grant to RAS). Constructive reviews by Sue Cashman and an anonymous reviewer are greatly appreciated.

References

Antonellini, M., Aydin, A., 1995. Effect of faulting on fluid flow in porous sandstones: geometry and spatial distribution. American Association of Petroleum Geologists Bulletin 79, 642–671.

Aydin, A., Borja, R.I., Eichhubl, P., 2006. Geological and mathematical framework for failure modes in granular rock. Journal of Structural Geology 28, 83–98.

Baud, P., Klein, E., Wong, T.-F., 2004. Compaction localization in porous sandstones: spatial evolution of damage and acoustic emission activity. Journal of Structural Geology 26, 603–624.

Baud, P., Vajdova, V., Wong, T.-F., 2006. Shear-enhanced compaction and strain localization: inelastic deformation and constitutive modeling of four porous sandstones. Journal of Geophysical Research 111, B12401. doi:10.1029/2005JB004101.

Baxevanis, T., Papamichos, E., Flornes, O., Larsen, I., 2006. Compaction bands and induced permeability reduction in Tuffeau de Maastricht calcarenite. Acta Geotechnica 1, 123–135.

Bjørkum, P.A., Oelkers, E.H., Nadeau, P.H., Walderhaug, O., Murphy, W.M., 1998. Porosity prediction in quartzose sandstones as a function of time, temperature, depth, stylolite frequency, and hydrocarbon saturation. American Association of Petroleum Geologists Bulletin 82, 637–648.

Blakey, R.C., Peterson, F., Kocurek, G., 1988. Synthesis of late Paleozoic and Mesozoic eolian deposits of the Western Interior of the United States. Sedimentary Geology 56, 3–125.

Cobbold, P.R., 1977. Description and origin of banded deformation structures. I. Regional strain, local perturbations and deformation bands. Canadian Journal of Earth Science 14, 1721–1731.

Davis, G.H., 1999. Structural geology of the Colorado Plateau Region of southern Utah. In: Geological Society of America Special Paper, vol. 342 1–157.

Davis, G.H., Bump, A.P., 2009. Structural geologic evolution of the Colorado Plateau. In: Kay, S.M., Ramos, V.A., Dickinson, W.R. (Eds.), Backbone of the Americas: Shallow Subduction, Plateau Uplift, and Ridge and Terrane Collision. Geological Society of America Memoir, vol. 204, pp. 99–124.

Dickinson, W.R., 2009. Anatomy and global context of the North American Cordillera. In: Kay, S.M., Ramos, V.A., Dickinson, W.R. (Eds.), Backbone of the Americas: Shallow Subduction, Plateau Uplift, and Ridge and Terrane Collision. Geological Society of America Memoir, vol. 204, pp. 1–29.

DiGiovanni, A.A., Fredrich, J.T., Holcomb, D.J., Olsson, W.A., 2007. Microscale damage evolution in compacting sandstone. In: Lewis, H., Couples, G.D. (Eds.), The Relationship Between Damage and Localization. Geological Society Special Publication, vol. 289, pp. 89–103.

Doelling, H.H., Willis, G.C., 2006. Geologic Map of the Smoky Mountain 30′×60′ Quadrangle, Kane and San Juan Counties, Utah, and Coconino County, Arizona. Utah Geological Survey.

Eichhubl, P., Taylor, W.L., Pollard, D.D., Aydin, A., 2004. Paleo-fluid flow and deformation in the Aztec Sandstone at the Valley of Fire, Nevada—evidence for the coupling of hydrogeologic, diagenetic, and tectonic processes. Geological Society of America Bulletin 116, 1120–1136.

Eichhubl, P., Hooker, J., Laubach, S.E., 2010. Pure and shear-enhanced compaction bands in Aztec Sandstone. Journal of Structural Geology 32, 1873–1886.

Fortin, J., Stanchits, S., Dresen, G., Gueguen, Y., 2009. Acoustic emissions monitoring during inelastic deformation of porous sandstone: comparison of three modes of deformation. Pure and Applied Geophysics 166, 823–841.

Fossen, H., 2010a. Deformation bands formed during soft-sediment deformation: observations from SE Utah. Marine and Petroleum Geology 27, 215–222.

Fossen, H., 2010b. Structural Geology. Cambridge University Press, Cambridge. 463 p.

Fossen, H., Bale, A., 2007. Deformation bands and their influence on fluid flow. American Association of Petroleum Geologists Bulletin 91, 1685–1700.

Fossen, H., Schultz, R.A., Shipton, Z.K., Mair, K., 2007. Deformation bands in sandstone – a review. Journal of the Geological Society, London 164, 755–769.

Friedman, M., Logan, J.M., 1973. Lüders' bands in experimentally deformed sandstone and limestone. Geological Society of America Bulletin 84, 1465–1476.

Goldstrand, P.M., 1994. Tectonic development of Upper Cretaceous to Eocene strata of southwestern Utah. Geological Society of America Bulletin 106, 145–154.

Grueschow, E., Rudnicki, J.W., 2005. Elliptic yield cap constitutive modeling for high porosity sandstone. International Journal of Solids and Structures 42, 4574–4587.

Haimson, B.C., 2001. Fracture-like borehole breakouts in high-porosity sandstone: are they caused by compaction bands? Physics and Chemistry of the Earth 26, 15–20.

Haimson, B., Lee, H., 2004. Borehole breakouts and compaction bands in two high-porosity sandstones. International Journal of Rock Mechanics and Mining Science 41, 287–301.

Holcomb, D.J., Rudnicki, J.W., Issen, K., Sternlof, K., 2007. Compaction localization in the Earth and the laboratory: state of the research and research directions. Acta Geotechnica 2, 1–15. doi:10.1007/s11440-007-0027-y.

Issen, K.A., Rudnicki, J.W., 2000. Conditions for compaction bands in porous rock. Journal of Geophysical Research 105, 21529–21536.

Kong, M., Bharracharya, R.N., James, C., Batsu, A., 2005. A statistical approach to estimate the 3D size distribution of spheres from 2D size distributions. Geological Society of America Bulletin 117, 244–249.

Marketos, G., Bolton, M.D., 2009. Compaction bands simulated in discrete element models. Journal of Structural Geology 31, 479–490.

Mollema, P.N., Antonellini, M.A., 1996. Compaction bands: a structural analog for anti-mode I cracks in aeolian sandstone. Tectonophysics 267, 209–228.

Moore, D.W., Straub, A.W., 2001. Correlation of upper Cretaceous and Paleogene(?) rocks beneath the Claron Formation, Crow Creek, western Markagunt Plateau, Southwest Utah. In: The Geologic Transition, High Plateaus to Great Basin: A symposium and field guide. The Mackin, vol. 30. Utah Geological Association, Salt Lake City, pp. 75–95.

Okubo, C.H., Schultz, R.A., 2007. Compactional deformation bands in Wingate Sandstone; additional evidence of an impact origin for Upheaval Dome, Utah. Earth and Planetary Science Letters 256, 169–181.

Olsson, W.A., 1999. Theoretical and experimental investigation of compaction bands in porous rock. Journal of Geophysical Research 104, 7219–7228.

Olsson, W.A., 2000. Origin of Lüders' bands in deformed rock. Journal of Geophysical Research-Solid Earth 105 (B3), 5931–5938.

Roberts, E.M., Deino, A.L., Chan, M.A., 2005. $^{40}Ar/^{39}Ar$ age of the Kaiparowits Formation, southern Utah, and correlation of contemporaneous Campanian strata and vertebrate faunas along the margin of the Western Interior Basin. Cretaceous Research 26, 307–318.

Rotevatn, A., Torabi, A., Fossen, H., Braathen, A., 2008. Slipped deformation bands: a new type of cataclastic deformation bands in Western Sinai, Suez rift, Egypt. Journal of Structural Geology 30, 1317–1331.

Saillet, E., 2009. La localisation de la déformation dans les grés poreux: caractérisation d'un analogue de réservoir gréseux et faillé dans le Bassin du Sud-Est, Provence, France. Unpublished Docteur en Sciences thesis. University de Nice-Sophia Antipolis.

Saillet, E., Wibberley, C.A.J., 2010. Evolution of cataclastic faulting in high-porosity sandstone, Bassin du Sud-Est, Provence, France. Journal of Structural Geology 32, 1590–1608.

Schultz, R.A., 2009. Scaling and paleodepth of compaction bands, Nevada and Utah. Journal of Geophysical Research 114, 13. doi:10.1029/2008JB005876.

Schultz, R.A., 2011. Relationship of compaction bands in Utah to Laramide fault-relatedfolding. Earth and Planetary Science Letters 304, 29–35.

Schultz, R.A., Siddharthan, R., 2005. A general framework for the occurrence and faulting of deformation bands in porous granular rocks. Tectonophysics 411, 1–18.

Schultz, R.A., Okubo, C.H., Fossen, H., 2010. Porosity and grain size controls on compaction band formation in Jurassic Navajo Sandstone. Geophysical Research Letters 37, L22306. doi:10.1029/2010GL044909.

Stanchits, S., Fortin, J., Gueguen, Y., Dresen, G., 2009. Initiation and propagation of compaction bands in dry and wet Bentheim Sandstone. Pure and Applied Geophysics 166, 843–868.

Sternlof, K., Karimi-Fard, M., Durlofsky, L.J., 2006. Flow and transport effects of compaction bands in sandstone at scales relevant to aquifer and reservoir management. Water Resources Research 42, W07425. doi:10.1029/2005WR004664.

Sternlof, K., Rudnicki, J.W., Pollard, D.D., 2005. Anticrack inclusion model for compaction bands in sandstone. Journal of Geophysical Research 110, B11403. doi:10.1029/2005JB003764.

Taylor, T.R., Giles, M.R., Hathon, L.A., Diggs, T.N., Braunsdorf, N.R., Birbiglia, G.V., Kittridge, M.G., Macaulay, C.I., Espejo, I.S., 2010. Sandstone diagenesis and reservoir quality prediction: models, myths, and reality. American Association of Petroleum Geologists Bulletin 94, 1093–1132.

Tembe, S., Baud, P., Wong, T.-F., 2008. Stress conditions for the propagation of discrete compaction bands in porous sandstone. Journal of Geophysical Research 113, B02409. doi:10.1029/2005JB003611.

Tindall, S.E., Davis, G.H., 1999. Monocline development by oblique-slip fault-propagation folding: the East Kaibab monocline, Colorado Plateau, Utah. Journal of Structural Geology 21, 1303–1320.

Tindall, S.E., Storm, L.P., Jenesky, T.A., Simpson, E.L., 2010. Growth faults in the Kaiparowits Basin, Utah, pinpoint initial Laramide deformation in the western Colorado Plateau. Lithosphere 2, 221–231.

Torabi, A., Fossen, H., Alaei, B., 2008. Application of spatial correlation functions in permeability estimation of deformation bands in porous rocks. Journal of Geophysical Research 113, B08208. doi:10.1029/2007JB005455.

Townend, E., Thompson, B.D., Benson, P.M., Meredith, P.G., Baud, P., Young, R.P., 2008. Imaging compaction band propagation in Diemelstadt sandstone using acoustic emission locations. Geophysical Research Letters 35, L15301. doi:10.1029/2008GL034723.

Vardoulakis, I., Sulem, J., 1995. Bifurcation Analysis in Geomechanics. Blackie Academic, Glasgow.

Wibberley, C.A.J., Petit, J.-P., Rives, T., 2007. The mechanics of fault distribution and localization in high-porosity sands, Provence, France. In: Lewis, H., Couples, G.D. (Eds.), The relationship between damage and localization. Geological Society, London, Special Publications, vol. 164, pp. 599–608.

Wong, T.-f., David, C., Zhu, W., 1997. The transition from brittle faulting to cataclastic flow in porous sandstones: mechanical deformation. Journal of Geophysical Research 102, 3009–3025.

Zhang, J., Wong, T.-F., Davis, D.M., 1990. Micromechanics of pressure-induced grain crushing in porous rocks. Journal of Geophysical Research 95, 341–352.